



OPEN

DATA DESCRIPTOR

A high-content image-based drug screen of clinical compounds against cell transmission of adenovirus

Fanny Georgi¹, Fabien Kuttler², Luca Murer¹, Vardan Andriasyan¹, Robert Witte¹, Artur Yakimovich^{3,4}, Gerardo Turcatti² & Urs F. Greber¹✉

Human adenoviruses (HAdVs) are fatal to immuno-suppressed individuals, but no effective anti-HAdV therapy is available. Here, we present a novel image-based high-throughput screening (HTS) platform, which scores the full viral replication cycle from virus entry to dissemination of progeny and second-round infections. We analysed 1,280 small molecular weight compounds of the Prestwick Chemical Library (PCL) for interference with HAdV-C2 infection in a quadruplicate, blinded format, and performed robust image analyses and hit filtering. We present the entire set of the screening data including all images, image analyses and data processing pipelines. The data are made available at the Image Data Resource (IDR, idr0081). Our screen identified Nelfinavir mesylate as an inhibitor of HAdV-C2 multi-round plaque formation, but not single round infection. Nelfinavir has been FDA-approved for anti-retroviral therapy in humans. Our results underscore the power of image-based full cycle infection assays in identifying viral inhibitors with clinical potential.

Background & Summary

Human adenoviruses (HAdVs) affect the respiratory, urinary and gastrointestinal tracts and the eyes. They cause morbidity and mortality, especially to immuno-compromised patients^{1,2} as indicated by a recent outbreak in the USA killing 12 children, or a recent case of meningoencephalitis in a middle-aged woman in the USA³. HAdVs have a high prevalence⁴⁻⁷ and are broadly used as gene therapy and vaccination vectors as well as oncolytic viruses⁸⁻¹⁰. The high seroprevalence of HAdV-C2 and C5 (species C, types 2 and 5) underlines that HAdV infections are asymptomatic in healthy individuals, but persist in mucosal lymphocytes, and thereby pose a risk for immunosuppressed patients undergoing stem cell transplantation^{11,12}. More than 100 HAdV genotypes are grouped into seven species based on hemagglutination assays and genome sequences^{13,14}. Types of the species A, F and G replicate in the gastrointestinal tract, B, C and E in the respiratory tract, and B and D in the conjunctiva of the eyes. Notably, species B members have a broad tropism, including kidney and hematopoietic cells^{6,12}.

HAdV has a double-stranded DNA genome of ~36 kbp tightly packaged into an icosahedral protein capsid of about 90 nm in diameter^{15,16}. HAdV-C2 and C5 enter cells by receptor-mediated endocytosis, shed minor capsid proteins, expose the membrane lytic protein, penetrate the endosomal membrane and are transported to the nuclear membrane, where they uncoat and release their genome to the nucleus¹⁷⁻²⁰. In the nucleus, the viral genome gives rise to the immediate early viral mRNA encoding the E1A protein, which transactivates the subviral promoters, drives lytic infection and maintains genome persistence in presence of interferon²¹⁻²³. Proteolytically matured HAdV progeny is released upon rupture of the nuclear envelope and the plasma membrane²⁴⁻²⁶.

Currently, there is no effective therapy available against HAdV disease. The standard of care is the nucleoside analogue Cidofovir, with poor clinical efficacy^{6,27}. The problem is exacerbated by the shortage of a suitable small animal model for HAdV disease, although Syrian Hamsters are susceptible to HAdV-C infection and give rise to

¹Department of Molecular Life Sciences, University of Zurich (UZH), Winterthurerstrasse, 190, 8057, Zurich, Switzerland. ²Biomolecular Screening Facility, School of Life Sciences, Ecole Polytechnique Fédérale de Lausanne (EPFL), Station 15, Lausanne, 1015, Switzerland. ³MRC Laboratory for Molecular Cell Biology, University College London, Gower St, London, WC1E 6BT, United Kingdom. ⁴Artificial Intelligence for Life Sciences CIC, 40 Gowers walk, London, E1 8BH, United Kingdom. ✉e-mail: urs.greber@mls.uzh.ch

viral progeny²⁸. Here, we developed an image-based procedure to identify novel inhibitors of HAdV infection in cell culture. We used the commercially available Prestwick Chemical Library (PCL) comprising 1,280 off-patent mostly FDA-approved small molecules (listed in PCL compounds tested in the screening procedure²⁹). The PCL comprises compounds against diseases including infection and cancer^{30,31}, collected at prestwickchemical.com/libraries-publications.

We performed a phenotypic screen against HAdV-C2 infection employing automated fluorescence microscopy and image-based scoring of the progression of multi-round infections using the Plaque2.0 software³² (Fig. 1a,b). For representative images in 384 well plates, see Fig. 1c. The procedure features robust imaging, image analysis and data processing, as concluded from two parallel workflows carried out at independent institutions, the Department of Molecular Life Sciences at University of Zurich (UZH), and the Biomolecular Screening Facility at Ecole Polytechnique Fédérale de Lausanne (EPFL).

Five phenotypic features scored the effects of the compounds on HAdV-C2-dE3B-GFP-infected human lung cancer epithelial A549 cells – the number of infected and uninfected cell nuclei, the infection index (infected nuclei per total nuclei), the number of plaques (areas of infection foci originating from a single productively infected cell as in non-perturbed infections depicted in Fig. 1d, left image) and the integrated signal of the infection marker green fluorescence protein (GFP) encoded in the reporter virus genome. All data are available at the Image Data Resource (IDR, idr.openmicroscopy.org), IDR accession number [idr0081](https://doi.org/10.21969/openmicroscopy.idr0081)³³, and can be accessed via the IDR web client. Raw and scored infection phenotypes are provided for UZH and EPFL analyses. Rigorous assay development ensured a high data quality, as indicated by mean Z' -factors of 0.52 for the plaque numbers. The screening was performed in four biological replicates at high reproducibility. Compounds that gave significant toxicity in uninfected cells were excluded during hit filtering.

Imaging, image analysis and scoring by the two independent teams yielded well correlated data and a congruent list of top hits, provided in Table 1. We identified Nelfinavir mesylate (Nelfinavir in short) as best inhibitor of HAdV infection. As evident in representative images presented in Fig. 1d, Nelfinavir abolishes the formation of plaques, but not single first round infections. We confirmed the antiviral efficacy of Nelfinavir in a follow-up study³⁴.

Methods

Virus. HAdV-C2-dE3B-GFP was produced as described²⁴ and fully sequenced³⁵. In brief, the virus was generated by exchange of the viral E3B genome region with a reporter cassette harbouring the enhanced green fluorescent protein (GFP) under the immediate early Cytomegalovirus (CMV) promoter²⁴. The virus was grown in A549 cells and purified by double caesium chloride gradient centrifugation³⁶. Aliquots supplemented with 10% glycerol (v/v) were stored at -80°C . HAdV-C2-dE3B-GFP was found to be homogeneous by SDS-PAGE and negative-stain analyses by transmission electron microscopy.

Cell culture. A549 (human adenocarcinomic alveolar basal epithelium) cells were obtained from the American Type Culture Collection (ATCC), Manassas, USA. The cells were maintained in full medium: high glucose Dulbecco Modified Eagle Medium (DMEM; Thermo Fisher Scientific, Waltham, USA) containing 7.5% fetal bovine serum (FBS, Invitrogen, Carlsbad, USA), 1% L-glutamine (Sigma-Aldrich, St. Louis, USA) and 1% penicillin streptomycin (Sigma-Aldrich, St. Louis, USA) and subcultured following PBS washing and trypsinisation (Trypsin-EDTA, Sigma-Aldrich, St. Louis, USA) weekly. Cells were grown at standard conditions (37°C , 5% CO_2 , 95% humidity) and passage number kept below 20.

Preparation of pre-plates. Ten μl 0.0125% DMSO in PBS was spotted on all 384 wells each of imaging-compatible 384-well plates (Matrix plates #4332, Thermo Fisher Scientific, Waltham, USA) using a Matrix WellMate dispenser and normal bore Matrix WellMate tubing cartridges (Thermo Fisher Scientific, Waltham, USA). Plates were sealed and stored at -20°C .

Blinding. The PCL compound arrangement as dispensed by EPFL in four subset plates A - D comprising each screening set replicate 1–4 was blinded and replaced by UZH with internal identifier (Raw Plaque-2.0 infection scores of the PCL screen, imaged and analysed at UZH and Processed Plaque-2.0 infection scores of the PCL screen, imaged and analysed at UZH²⁹, *compoundIdentifier* 1 to 1280). The identity of the compounds was only disclosed after the screening process and hit filtering (Raw Plaque-2.0 infection scores of the PCL screen, imaged and analysed at UZH and Processed Plaque-2.0 infection scores of the PCL screen, imaged and analysed at UZH²⁹ and Table 1, *PCL_ID* Prestw-1 to Prestw-1804 and *compoundName*).

Compounds. The PCL was obtained from Prestwick Chemical (Illkirch, France). 3'-deoxy-3'-fluorothymidine (DFT, CAS number 25526-93-6) was obtained from Toronto Research Chemical, North York, Canada. All compounds were dissolved in dimethyl sulfoxide (DMSO, Sigma-Aldrich, St. Louis, USA) at a final stock concentration of 10 mM and stored at -20°C .

PrestoBlue toxicity assay. Toxicity of the PCL compounds on uninfected A549 cells was assessed using the PrestoBlue Cell Viability reagent (Thermo Fisher Scientific, Waltham, USA). PrestoBlue^{37,38} is a cell viability and cytotoxicity indicator based on resazurin. Resazurin is reduced to resorufin in cellular respiration by accepting electrons from NADPH, FADH, FMNH, NADH and cytochromes. This reduction causes PrestoBlue to change from a non-fluorescent to a strongly fluorescent form. The conversion of PrestoBlue is proportional to the number of metabolically active cells and can be evaluated quantitatively using fluorescence or absorbance measurements. Briefly, following 3.5-day continuous treatment of A549 cells with compounds at concentrations and cell densities as in the screening protocol, 10% final PrestoBlue was added to each well and incubated for 1 h at standard cell incubation conditions. Fluorescence intensity (bottom-read) was measured using a multi-well plate reader (Tecan

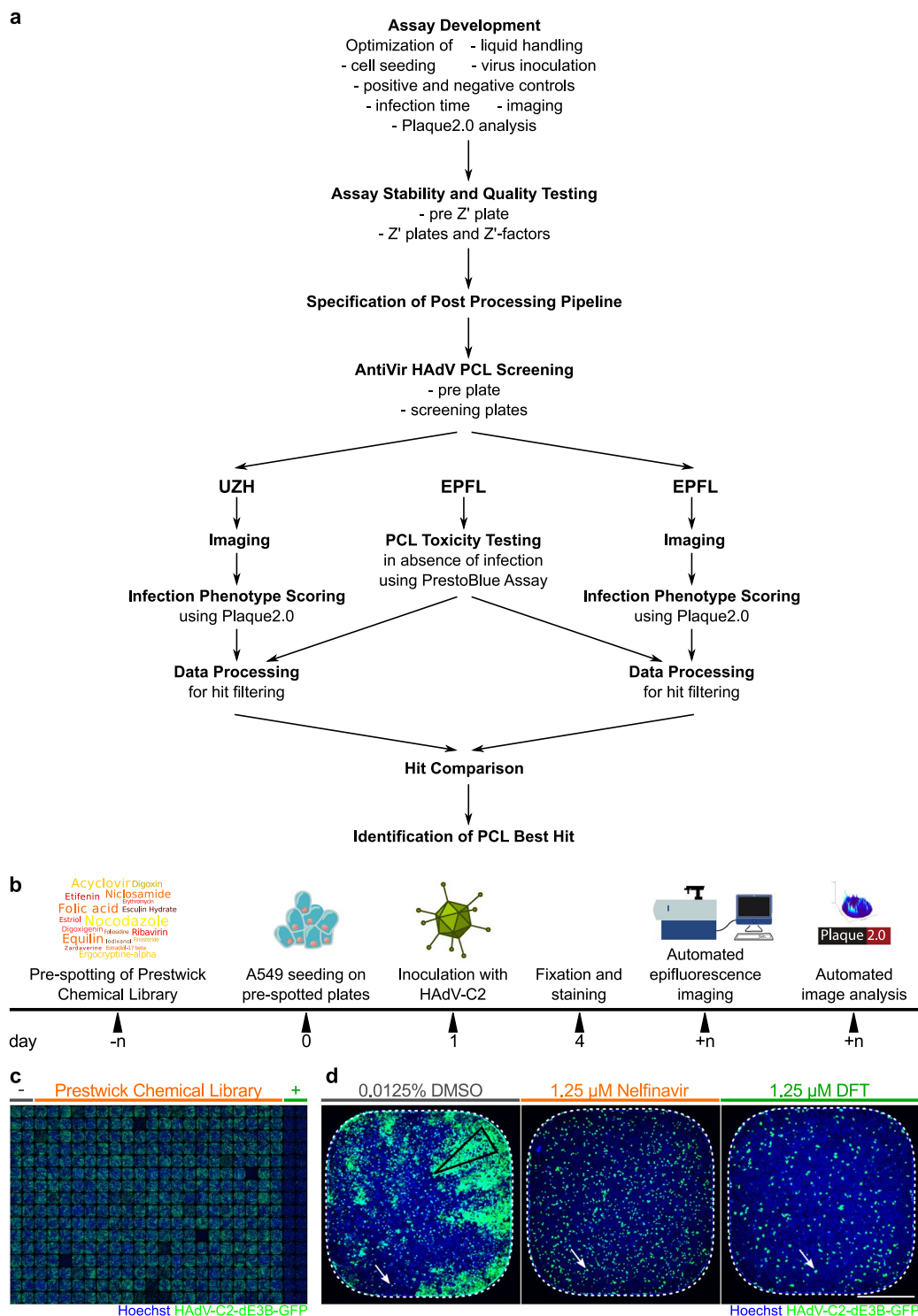


Fig. 1 The compound screening procedure. **(a)** Following assay development, stability and quality testing, the screening of the PCL against HAdV infection was performed. Imaging, image analysis and data processing were independently carried out at UZH and EPFL, before hit ranking. **(b)** Schematic overview of the wet-lab pipeline. PCL compounds and DFT positive control in DMSO as well as DMSO alone as negative control were pre-spotted onto 384-well imaging plates by Echo acoustic liquid handling at 10 nl corresponding to a final concentration of 1.25 μM in 80 μl assay volume/well and stored at -20 °C. Compound-blinded plates are thawed and 4,000 A549 cells/wells seeded. The following day, the cells were inoculated with HAdV-C2-dE3B at 1.77×10^5 genome equivalents/well. Allowing for multiple viral replication rounds, the cells were PFA-fixed at 72 hpi and the nuclei stained with Hoechst 33342. The infection phenotypes were imaged using an epifluorescence HT microscope and scored using Plaque2.0. The data of the four technical replicates were further processed in R or through EPFL-BSF LIMS. **(c)** Exemplary epifluorescence microscopy images of cells in 384-wells stitched to a screening plate overview of 32 replicates of negative (two most left columns) and positive control (two most

right columns) and 320 blinded PCL compounds (centre 20 columns). Hoechst-stained nuclei are shown in blue, viral GFP in green. **(d)** Representative 384-well epifluorescence microscopy images of the DMSO negative control (most left), the DFT positive control (most right) and the top hit Nelfinavir mesylate (centre). Empty black triangle indicates a plaque (infection focus) from a productively infected cell. White arrows point out infected cells that did not form a plaque. Hoechst-stained nuclei are shown in blue, infected cells expressing GFP in green. Scale bar is 5 mm.

| | | UZH | | | | |
|-----------|-------|------------------|---------------------------|-----------------|-------------------|-----------------------|
| | | 3 sigma | | | | |
| Barcode | Plate | number Of Nuclei | number Of Infected Nuclei | infection Index | number Of Plaques | total Virus Intensity |
| BSF018104 | Za | -1.11 | 0.50 | 0.57 | 0.50 | 0.07 |
| BSF018105 | Zb | -8.10 | 0.30 | 0.45 | 0.39 | -0.07 |
| Mean | | -4.61 | 0.40 | 0.51 | 0.44 | 0.00 |
| | | UZH | | | | |
| | | 2 sigma | | | | |
| Barcode | Plate | number Of Nuclei | number Of Infected Nuclei | infection Index | number Of Plaques | total Virus Intensity |
| BSF018104 | Za | -0.41 | 0.67 | 0.71 | 0.67 | 0.07 |
| BSF018105 | Zb | -5.07 | 0.53 | 0.63 | 0.59 | -0.07 |
| Mean | | -2.74 | 0.60 | 0.67 | 0.63 | 0.00 |
| | | EPFL | | | | |
| | | 3 sigma | | | | |
| Barcode | Plate | number Of Nuclei | number Of Infected Nuclei | infection Index | number Of Plaques | total Virus Intensity |
| BSF018104 | Za | -1.20 | 0.36 | 0.47 | 0.52 | 0.08 |
| BSF018105 | Zb | -1.23 | 0.27 | 0.32 | 0.44 | -0.04 |
| Mean | | -1.22 | 0.32 | 0.40 | 0.48 | 0.02 |
| | | EPFL | | | | |
| | | 2 sigma | | | | |
| Barcode | Plate | number Of Nuclei | number Of Infected Nuclei | infection Index | number Of Plaques | total Virus Intensity |
| BSF018104 | Za | -0.47 | 0.58 | 0.64 | 0.68 | 0.38 |
| BSF018105 | Zb | -0.49 | 0.52 | 0.55 | 0.63 | 0.31 |
| Mean | | -0.48 | 0.55 | 0.60 | 0.66 | 0.35 |

Table 1. Summary of screening controls and top hits. Mean corresponds to the means over four biological replicates of PCL compound and 16 biological replicates each carrying 32 technical replicates for each control. Neg. ctr. refers to solvent control (DMSO), pos. ctr. to DFT-treated wells. Normalized indicates the mean read-outs of each compound relative to the mean of the positive control over all replicates. Toxicity was accessed by PrestoBlue assay of 3.5-day treatment of uninfected A549 cells as well as by the nuclei Z'-factor in the screen. Hits were selected for low toxicity and high inhibitory effects compared to solvent control samples. Note that compounds were scored toxic, if they showed significant toxicity in either of the assays.

Infinite F500, Tecan, Männedorf, Switzerland) with excitation at 560/10 nm, emission at 590/10 nm at a fixed gain. Doxorubicin hydrochloride (Prestw-438, Prestwick Chemical, Illkirch, France) was used as a positive control for cytotoxicity, at a final concentration of 10 μ M, and the corresponding concentration of the drug solvent DMSO was used as a negative control. The full PCL library was tested on duplicated plates. The EPFL-BSF in-house Laboratory Information Management System (LIMS) was used for data processing and statistical validation. First, raw PrestoBlue readings were normalized per plate to negative control values at 0 and positive controls at 1. Then, the normalized values of both duplicates were averaged. Assay quality was assessed for each plate through the Z'-factor calculation. Compounds were considered toxic, when the normalized value for all replicates was higher than the average + 3 σ (standard deviation, SD) of the DMSO negative control for the corresponding plate. Scores and score SD were then calculated for hit compounds by averaging normalized value for all replicates.

Preparation of plates for Z'-factor and drug screening. Ten nl of 10 mM PCL compounds, the nucleoside analogue DFT positive control (all dissolved in DMSO) and DMSO only as negative control were pre-spotted on imaging-compatible 384-well plates (Falcon plates, Corning Inc., New York, USA) using an Echo acoustic liquid handling system (Labcyte, San Jose, USA) by the EPFL-BSF, sealed and stored at -20 °C. Each Z'-factor 384-well plate consisted of 192 technical replicates of positive and negative controls, each. Each screening plate set consisted of four subset plates A to D. Each screening plate comprised 32 technical replicates of positive and negative controls, each, and 320 PCL compounds.

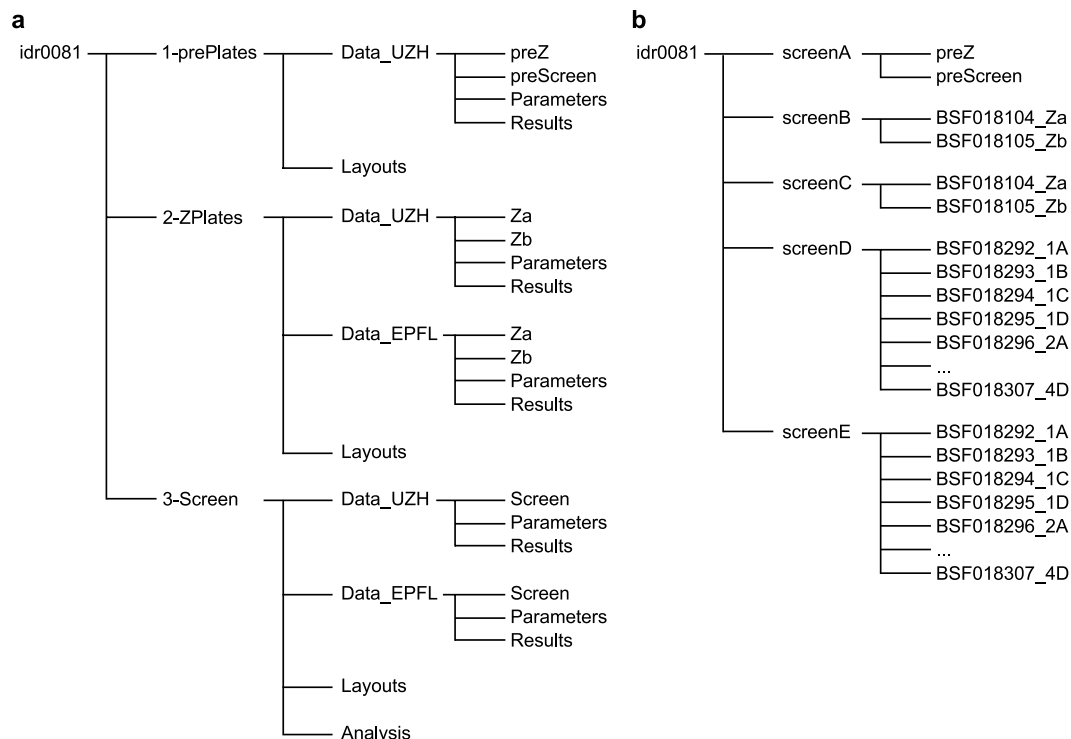


Fig. 2 Project data structure available at IDR, accession number idr0081³³. **(a)** In the data provided for download, there are three sub-folders for *1-prePlates*, *2-ZPlates* and *3-Screen*. The latter two contain both the images and analyses generated by UZH and EPFL. **(b)** The data provided for viewing are divided into five screens: *screenA* contains the pre-plates and *screenB* and *screenC* consist of the *Z'*-factor plates imaged and analysed at UZH and EPFL, respectively. *screenD* and *screenE* provide the screening data obtained at UZH and EPFL, respectively.

Wet-lab screening pipeline. The screening was performed in four independent biological replicates 1–4. Liquid handling was performed using a Matrix WellMate dispenser and Matrix WellMate tubing cartridges (Thermo Fisher Scientific, Waltham, USA). Prior to usage, tubings were rinsed with 125 ml autoclaved double-distilled (dd) H₂O followed by 125 ml autoclaved PBS. Pre-spotted compound plates were thawed at room temperature (RT) for 30 min, briefly centrifuged before compounds were dissolved in 10 μl/well of PBS. 4,000 A549 cells/well in 60 μl full medium were seeded onto the compounds using standard bore tubing cartridges. Following cell adhesion over night, the cells were inoculated with 1.77*10⁵ genome equivalents per well of HAdV-C2-dE3B-GFP in 10 μl of full medium using bovine serum albumin (BSA, cell-culture grade, Sigma-Aldrich, St. Louis, USA)-blocked small bore tubing cartridges. The final compound concentration was 1.25 μM at 0.0125% DMSO. Infection was allowed to progress over multiple infection rounds for 72 h giving rise to foci of infected cells originating from a single first round infected cell. Cells were fixed for 1 h at RT by addition of 26.6 μL 16% PFA and 4 μg/ml Hoechst 33342 (Sigma-Aldrich, St. Louis, USA) in PBS using standard bore tubing cartridges. Cells were washed three times with PBS before PBS supplemented with 0.02% N₃ was added and plates were sealed for long-term storage at 4 °C. Following usage, tubings were rinsed with 125 ml autoclaved ddH₂O followed by 125 ml autoclaved PBS and autoclaved for re-usage.

Imaging. Nuclei stained with Hoechst 33342 (DAPI channel) and viral GFP (FITC channel) were imaged on two devices. At UZH, plates were imaged on an IXM-C automated high-throughput fluorescence microscope (Molecular Devices, San Jose, USA) using MetaXpress (version 6.2, Molecular Devices, San Jose, USA) and a 4x air objective (Nikon S Fluor, 0.20 NA, 15.5 mm WD, Nikon Instruments, Minato, Japan) at widefield mode. Images of 2,048² px at 1.72 μm/px resolution were acquired on an Andor sCMOS camera (Oxford Instruments, Abingdon, UK). Exposure times: DAPI 150 ms, FITC 20 ms. At EPFL, images were acquired on a IN Cell 2200 automated high-throughput fluorescence microscope (GE Healthcare, Chicago, USA) using IN Cell Analyzer (version 6.2, GE Healthcare, Chicago, USA) and a 4x air objective (Nikon Plan Apo, 0.20 NA, 15.7 mm WD, Nikon Instruments, Minato, Japan) at widefield mode. Image size 2,048² px at 1.625 μm/px resolution acquired on an Andor sCMOS camera. Exposure times: DAPI 300 ms, FITC 40 ms.

Image analysis. The infection phenotype for each well was quantified by Plaque2.0³² (<https://github.com/plaque2/matlab/tree/antivir>) via five main read-outs: number of nuclei, number of infected nuclei, the ratio between infected and total nuclei referred to as infection index, number of multi-round infection foci termed plaques (plaque forming unit(s), pfu) and the integrated viral transgenic GFP intensity. Plaque2.0 parameters were optimized independently at UZH and EPFL for the data acquired at the respective institution. Well- and object-based read-outs are provided in the Plaque2.0 output files.

| Barcode | Plate | UZH | | | | | EPFL | | | | |
|-----------|-------|------------------|---------------------------|-----------------|-------------------|-----------------------|------------------|---------------------------|-----------------|-------------------|-----------------------|
| | | 3 sigma | | | | | 3 sigma | | | | |
| | | number Of Nuclei | number Of Infected Nuclei | infection Index | number Of Plaques | total Virus Intensity | number Of Nuclei | number Of Infected Nuclei | infection Index | number Of Plaques | total Virus Intensity |
| BSF018104 | Za | -1.11 | 0.50 | 0.57 | 0.50 | 0.07 | -1.20 | 0.36 | 0.47 | 0.52 | 0.08 |
| BSF018105 | Zb | -8.10 | 0.30 | 0.45 | 0.39 | -0.07 | -1.23 | 0.27 | 0.32 | 0.44 | -0.04 |
| Mean | | -4.61 | 0.40 | 0.51 | 0.44 | 0.00 | -1.22 | 0.32 | 0.40 | 0.48 | 0.02 |
| Barcode | Plate | UZH | | | | | EPFL | | | | |
| | | 2 sigma | | | | | 2 sigma | | | | |
| | | number Of Nuclei | number Of Infected Nuclei | infection Index | number Of Plaques | total Virus Intensity | number Of Nuclei | number Of Infected Nuclei | infection Index | number Of Plaques | total Virus Intensity |
| BSF018104 | Za | -0.41 | 0.67 | 0.71 | 0.67 | 0.07 | -0.47 | 0.58 | 0.64 | 0.68 | 0.38 |
| BSF018105 | Zb | -5.07 | 0.53 | 0.63 | 0.59 | -0.07 | -0.49 | 0.52 | 0.55 | 0.63 | 0.31 |
| Mean | | -2.74 | 0.60 | 0.67 | 0.63 | 0.00 | -0.48 | 0.55 | 0.60 | 0.66 | 0.35 |

Table 2. Z'-factor plates. The quality of the platform was assessed prior to screening of the PCL by two independent Z'-factor plates containing 192 technical replicates of both positive control (1.25 μM DFT) and solvent only control (0.0125% DMSO). Z'-factors for the five Plaque2.0 read-outs³² obtained by independent analysis at UZH and EPFL were calculated according to Eq. (1) for 3 and 2σ.

Z'-factor calculation. The Z'-factor was computed using R version 3.3.2³⁹ according to Eq. (1)

$$Z' = 1 - \frac{(3\sigma_+ + 3\sigma_-)}{|\mu_+ - \mu_-|} \quad (1)$$

where σ_+ is the SD of the positive control, σ_- is the SD of the negative control, μ_+ the mean of the positive control and μ_- the mean of the negative control.

Screening data processing. Plaque2.0 results were further processed and filtered. At UZH, results were processed in R version 3.3.2³⁹, EPFL used KNIME version 3.4.0⁴⁰ as well as the EPFL-BSF in-house LIMS. Mean infection scores over the five Plaque2.0 read-outs of the four biological replicates of each PCL compound and the 16 biological replicates containing 32 technical replicates of positive and negative control, each, were calculated. Each compound's scores were normalized by the mean score of the DMSO negative control of the respective plate. Only non-toxic, effective PCL compounds were considered as HAdV inhibitor candidates. Non-toxic compounds were filtered by applying an inclusive μ_+ (mean of the negative control) $\pm 2\sigma$ (SD of the negative control) threshold for number of nuclei. Efficacy was filtered by applying an excluding $\mu_+ \pm 3\sigma$ threshold for the infection scores (number of infected nuclei, infection index, number of plaques or integrated GFP intensity). Subsequently, compounds exhibiting significant toxicity to noninfected cells were excluded.

Data Records

Data structure and repositories. The screening data comprise the information collected during assay development, including stability, quality and screening of the PCL itself. The latter two were imaged on two different microscopes. We provide the parameters used for Plaque2.0 image analysis, and the code for the subsequent hit filtering in R. The data available for download at the IDR, accession number idr0081³³, are structured as outlined in Fig. 2a. For download instructions, see idr.openmicroscopy.org/about/download. Moreover, the data can be viewed conveniently on the IDR web client (idr.openmicroscopy.org/webclient), where it is structured as depicted in Fig. 2b. Additionally, an annotated list of the PCL compounds as well as raw and scored screening data are available on figshare²⁹ as.txt files.

Data sets and file types. The data provided for download consists of three data sets 1 to 3 (see Fig. 2a).
 - 1-*prePlates* contains layouts (.csv), images (.tif), Plaque2.0 image analysis parameters (.mat) and results (.csv) for the assay stability test plates performed at UZH prior to Z'-factor plates (*preZ*) and the screen (*preScreen*).
 - 2-*ZPlates* contains layouts (.csv), images (.tif), Plaque2.0 image analysis parameters (.mat) and results (.csv) for the two Z'-factor plates *a* and *b* as imaged and analysed at UZH (*Data_UZH*) and EPFL (*Data_EPFL*).
 - 3-*Screen* contains layouts (.csv), images (.tif), Plaque2.0 image analysis parameters (.mat) and results (.csv) for the 16 screening plates (four biological replicates 1–4, each consisting of a set of four subset plates A–D) as imaged and analysed at UZH (*Data_UZH*) and EPFL (*Data_EPFL*). Moreover, *Analysis* contains the Plaque2.0 batch processing (*AntiVir_batchprocessing.m*) and hit filtering pipeline (*AntiVir_hitfiltering.R*) used by UZH. *Analysis* also contains the PrestoBlue raw results (.csv) for toxicity in absence of infection.
 The data provided for browsing via the IDR web client are assembled into five screens A to E (see Fig. 2b).
 - idr0081-study.txt summarizes the overall study and the five screens that were performed.
 - *screenA* contains the assay stability test plates performed at UZH prior to Z'-factor plates (*preZ*) and the screen (*preScreen*). *idr0081-screenA-library.txt* provides thorough information on the tested compounds including PubChem identifiers and their plate layout. *idr0081-screenA-processed.txt* presents the results of the Plaque2.0-based image analysis. *idr0081-screenA-mean.txt* summarises the infection scores per pre plate.

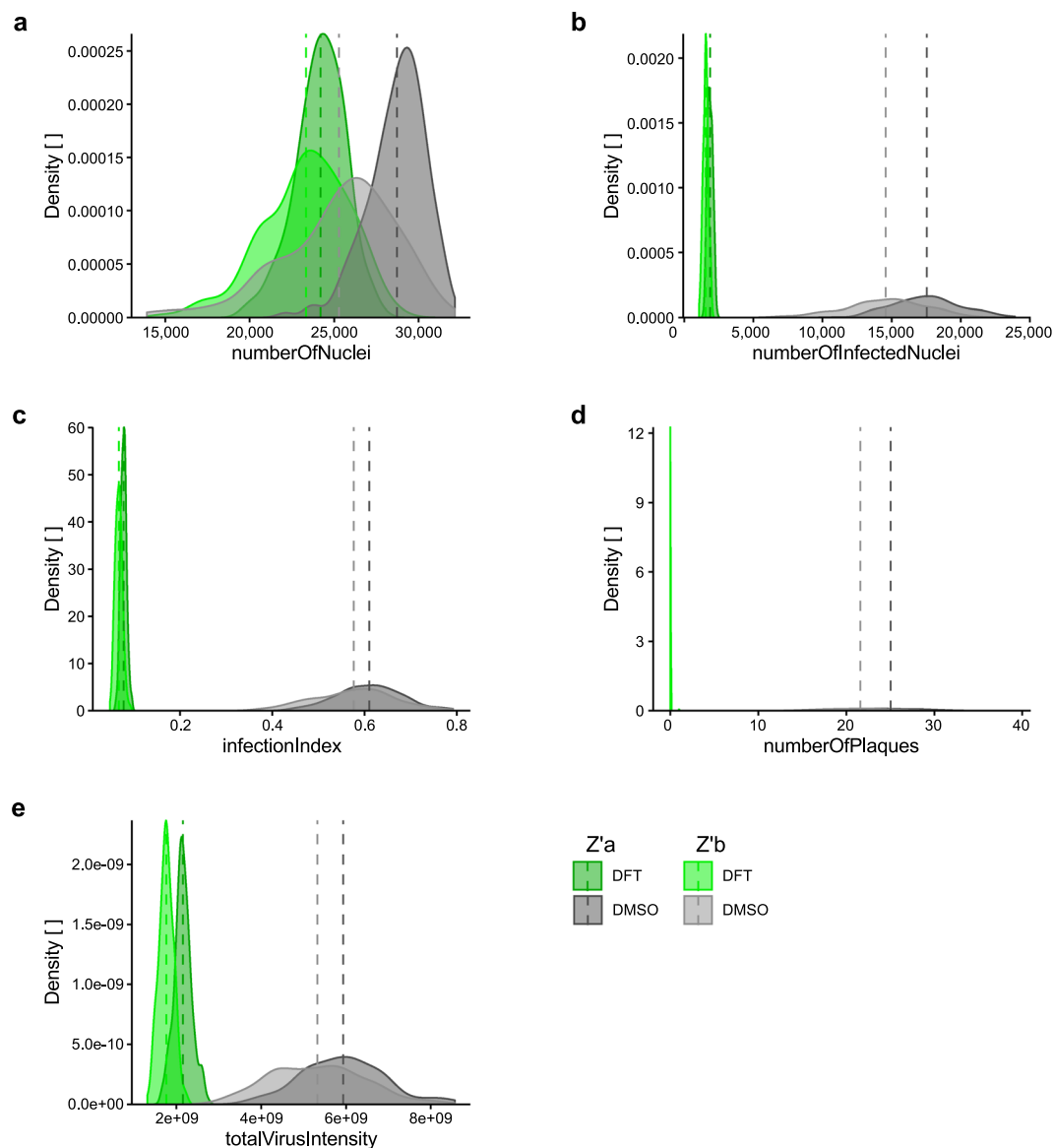


Fig. 3 Infection score density of positive and negative controls across Z' -factor plates. Distribution of (a) *numberOfNuclei*, (b) *numberOfInfectedNuclei*, (c) *infectionIndex*, (d) *numberOfPlaques* and (e) *totalVirusIntensity* in negative control (0.0125% DMSO) compared to positive control-treated (1.25 μ M DFT) samples of the two Z' -factor plates. Dark green and dark grey indicate Z' -factor plate a, light green and grey show Z' -factor plate b. Dashed vertical lines mark mean of 192 technical replicates.

- *screenB* contains the assay quality test plates (Z' -factor plates *a* and *b*) performed at UZH. *idr0081-screenB-library.txt* provides thorough information on the tested compounds including PubChem identifiers and their plate layout. *idr0081-screenB-processed.txt* presents the results of the Plaque2.0-based image analysis. *idr0081-screenB-mean.txt* summarises the infection scores per Z' -factor plate.

- *screenC* contains the assay quality test plates (Z' -factor plates *a* and *b*) performed at EPFL. *idr0081-screenC-library.txt* provides thorough information on the tested compounds including PubChem identifiers and their plate layout. *idr0081-screenC-processed.txt* presents the results of the Plaque2.0-based image analysis. *idr0081-screenC-mean.txt* summarises the infection scores per Z' -factor plate.

- *screenD* contains the PCL screening plates (in replicates 1 to 4, consisting of subset plates A to D) performed at UZH. *idr0081-screenD-library.txt* provides thorough information on the tested compounds including PubChem identifiers and their plate layout. *idr0081-screenD-processed.txt* presents the results of the Plaque2.0-based image analysis. *idr0081-screenB-filtered.txt* summarises the infection scores per compound and indicates if it was identified as hit.

- *screenE* contains the PCL screening plates (in replicates 1 to 4, consisting of subsets A to D) performed at EPFL. *idr0081-screenE-library.txt* provides thorough information on the tested compounds including PubChem identifiers and their plate layout. *idr0081-screenE-processed.txt* presents the results of the Plaque2.0-based image analysis. *idr0081-screenE-filtered.txt* summarises the infection scores per compound and indicates, if it was identified as hit.

| Barcode | Plate | UZH | | | | | EPFL | | | | |
|-----------|-------|------------------|---------------------------|-----------------|-------------------|----------------------|------------------|---------------------------|-----------------|-------------------|-----------------------|
| | | 3 sigma | | | | | 3 sigma | | | | |
| | | number Of Nuclei | number Of Infected Nuclei | infection Index | number Of Plaques | totalVirus Intensity | number Of Nuclei | number Of Infected Nuclei | infection Index | number Of Plaques | total Virus Intensity |
| BSF018292 | 1 A | -0.13 | 0.58 | 0.58 | 0.59 | 0.35 | -0.14 | 0.51 | 0.49 | 0.58 | 0.31 |
| BSF018293 | 1B | -0.88 | 0.58 | 0.65 | 0.55 | 0.34 | -0.35 | 0.51 | 0.52 | 0.51 | 0.35 |
| BSF018294 | 1 C | -1.01 | 0.62 | 0.62 | 0.63 | 0.33 | -0.74 | 0.52 | 0.50 | 0.66 | 0.32 |
| BSF018295 | 1D | -0.34 | 0.56 | 0.54 | 0.45 | 0.16 | -0.21 | 0.43 | 0.38 | 0.46 | 0.19 |
| BSF018296 | 2A | -1.35 | 0.64 | 0.67 | 0.55 | 0.30 | -0.20 | 0.57 | 0.55 | 0.55 | 0.28 |
| BSF018297 | 2B | -3.63 | 0.56 | 0.52 | 0.45 | 0.14 | -1.20 | 0.45 | 0.39 | 0.40 | 0.12 |
| BSF018298 | 2 C | -1.81 | 0.60 | 0.58 | 0.49 | 0.24 | -0.38 | 0.52 | 0.42 | 0.52 | 0.19 |
| BSF018299 | 2D | -1.94 | 0.57 | 0.57 | 0.57 | 0.24 | -0.22 | 0.50 | 0.43 | 0.63 | 0.20 |
| BSF018300 | 3 A | -1.74 | 0.64 | 0.66 | 0.56 | 0.36 | -0.54 | 0.55 | 0.51 | 0.59 | 0.34 |
| BSF018301 | 3B | -1.13 | 0.60 | 0.68 | 0.58 | 0.40 | -0.09 | 0.52 | 0.57 | 0.59 | 0.40 |
| BSF018302 | 3 C | -4.02 | 0.66 | 0.68 | 0.48 | 0.42 | -1.07 | 0.63 | 0.60 | 0.50 | 0.41 |
| BSF018303 | 3D | -2.36 | 0.55 | 0.63 | 0.51 | 0.36 | -0.10 | 0.58 | 0.54 | 0.52 | 0.35 |
| BSF018304 | 4A | -0.68 | 0.70 | 0.74 | 0.42 | 0.37 | -0.29 | 0.56 | 0.58 | 0.48 | 0.36 |
| BSF018305 | 4B | -0.17 | 0.71 | 0.74 | 0.51 | 0.50 | -0.50 | 0.63 | 0.67 | 0.50 | 0.50 |
| BSF018306 | 4 C | -0.44 | 0.61 | 0.62 | 0.50 | 0.28 | -0.28 | 0.50 | 0.48 | 0.47 | 0.26 |
| BSF018307 | 4D | -0.77 | 0.63 | 0.70 | 0.42 | 0.41 | -0.22 | 0.54 | 0.56 | 0.36 | 0.39 |
| Mean | | -1.40 | 0.61 | 0.64 | 0.52 | 0.32 | -0.41 | 0.53 | 0.51 | 0.52 | 0.31 |

Table 3. Z'-factors of screening plates. The quality of the screening data was assessed for each screening plate based on the 32 technical replicates of both positive control (1.25 μ M DFT) and solvent only control (0.0125% DMSO) in each plate. Z'-factors for the five Plaque2.0 read-outs³² obtained by independent analysis at UZH and EPFL were calculated according to Eq. (1) for 3σ .

Technical Validation

Assay stability. The wet-lab screening pipeline was optimized regarding liquid handling, cell seeding, virus inoculum, positive and negative controls, infection time, as well as imaging and image analysis. This ensured a high assay stability and reproducibility. Furthermore, all compounds, especially media and supplements, the BSA for tubing saturation, PFA- and Hoechst-supplemented fixative were prepared as large batch from a single lot and stored as single-use aliquots. Prior to every experiment, assay stability with respect to cell and infection phenotype was tested on pre-plates according to the established wet-lab, imaging and image analysis pipeline. Since the solvent control had already been spotted in 10 μ l PBS, no further PBS was added prior to cell seeding. Periodically, the virus stock dilution was tested and adjusted for experiments if necessary.

Assay quality determination: Z'-factor. The accuracy of the wet-lab, imaging and image analysis pipeline was assessed by two independently imaged and analysed Z'-factor plates (Table 2 and Fig. 3). 3σ Z'-factors of *numberOfInfectedNuclei*, *infectionIndex* and *numberOfPlaques* were in the range of 0.30 to 0.57, scoring good to excellent. *totalVirusIntensity* (Z'-factors between -0.07 to 0.08) were not suitable to identify HAdV infection inhibitors, while *numberOfNuclei* (Z'-factors between -1.11 to -8.10) was not a useable readout either. Additionally, the Z'-factors were determined for each of the 16 screening plates (Table 3 and Fig. 4). 3σ Z'-factors of *numberOfInfectedNuclei*, *infectionIndex* and *numberOfPlaques* were in the range of 0.27 to 0.57, scoring good to excellent.

Independent analysis and filtering. Imaging, image analysis and screening data processing were performed by two independent research teams at UZH and EPFL, as depicted in Fig. 1. Raw and scored infection phenotypes are shown for UZH and EPFL analyses (Raw Plaque-2.0 infection scores of the PCL screen, imaged and analysed at UZH, Processed Plaque-2.0 infection scores of the PCL screen, imaged and analysed at UZH and Raw Plaque-2.0 infection scores of the PCL screen, imaged and analysed at EPFL, Processed Plaque-2.0 infection scores of the PCL screen, imaged and analysed at EPFL, respectively²⁹). Both dry-lab pipelines confirmed the high assay quality (Tables 2 and 3). During hit filtering, PCL compounds that gave significant toxicity in uninfected cells were excluded during hit filtering (Fig. 5, PCL compounds excluded due to toxicity in uninfected cells²⁹). As summarized in Fig. 6 left panel, both scores are strongly correlated with R^2 between 0.6870 and 0.9870. Both approaches yielded identical top scored compounds (Fig. 6, right panel), of which Prestw-1764, Nelfinavir mesylate, was the top hit.

Usage Notes

Five parameters were used to score the infection phenotype of each well: the number of nuclei (*numberOfNuclei*), number of infected nuclei (*numberOfInfectedNuclei*), the ratio between number of infected and total nuclei (*infectionIndex*), the number of multi-round infection foci termed plaques (*numberOfPlaques*) and the extend of viral GFP reporter expression as integrated GFP intensity *totalVirusIntensity*).

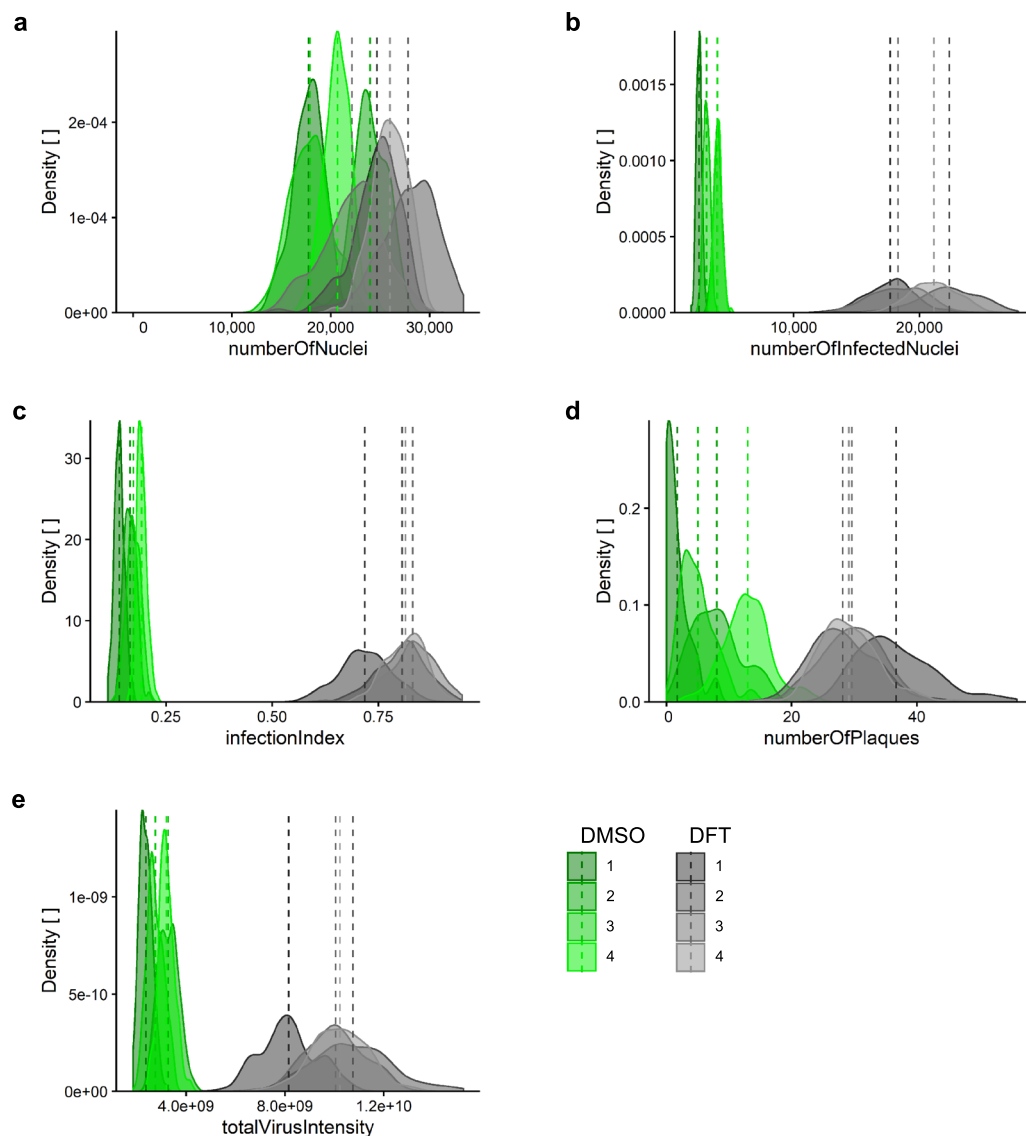


Fig. 4 Infection score density of positive and negative controls across screening replicates. Distribution of (a) *numberOfNuclei*, (b) *numberOfInfectedNuclei*, (c) *infectionIndex*, (d) *numberOfPlaques* and (e) *totalVirusIntensity* in negative control (0.0125% DMSO in grey) compared to positive control-treated (1.25 μ M DFT in green) samples of the screening sets. Replicates 1 to 4 indicated by colour shading are each comprised of four set plates containing 32 technical replicates per control. The dashed vertical lines indicate the corresponding mean values.

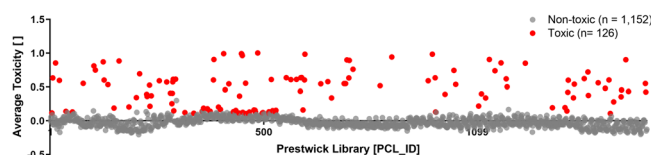


Fig. 5 PCL compound toxicity in uninfected cells. Of the 1,278 PCL compounds tested, 126 PCL compounds are found to be toxic, as shown in red, and listed in PCL compounds excluded due to toxicity in uninfected cells²⁹. A549 cells were treated with PCL compounds in duplicates according to the screening wet-lab protocol, however, in absence of HAdV infection for 3.5 days. Doxorubicin hydrochloride (Prestw-438) was used as a positive control for cytotoxicity, at a final concentration of 10 μ M, and the corresponding concentration of the drug solvent DMSO was used as a negative control. Cell viability was determined by PrestoBlue assay. PrestoBlue fluorescence intensities of each well were normalized per plate to negative control values at 0 and positive controls at 1. Compounds were considered toxic, when the normalized value for all replicates was higher than the average $+3\sigma$ (standard deviation, SD) of the DMSO negative control for the corresponding plate. X-axis indicates compounds by their PCL identifier (*PCL ID*, see PCL compounds tested in the screening procedure²⁹). Normalized average PrestoBlue read-outs are depicted on the y-axis.

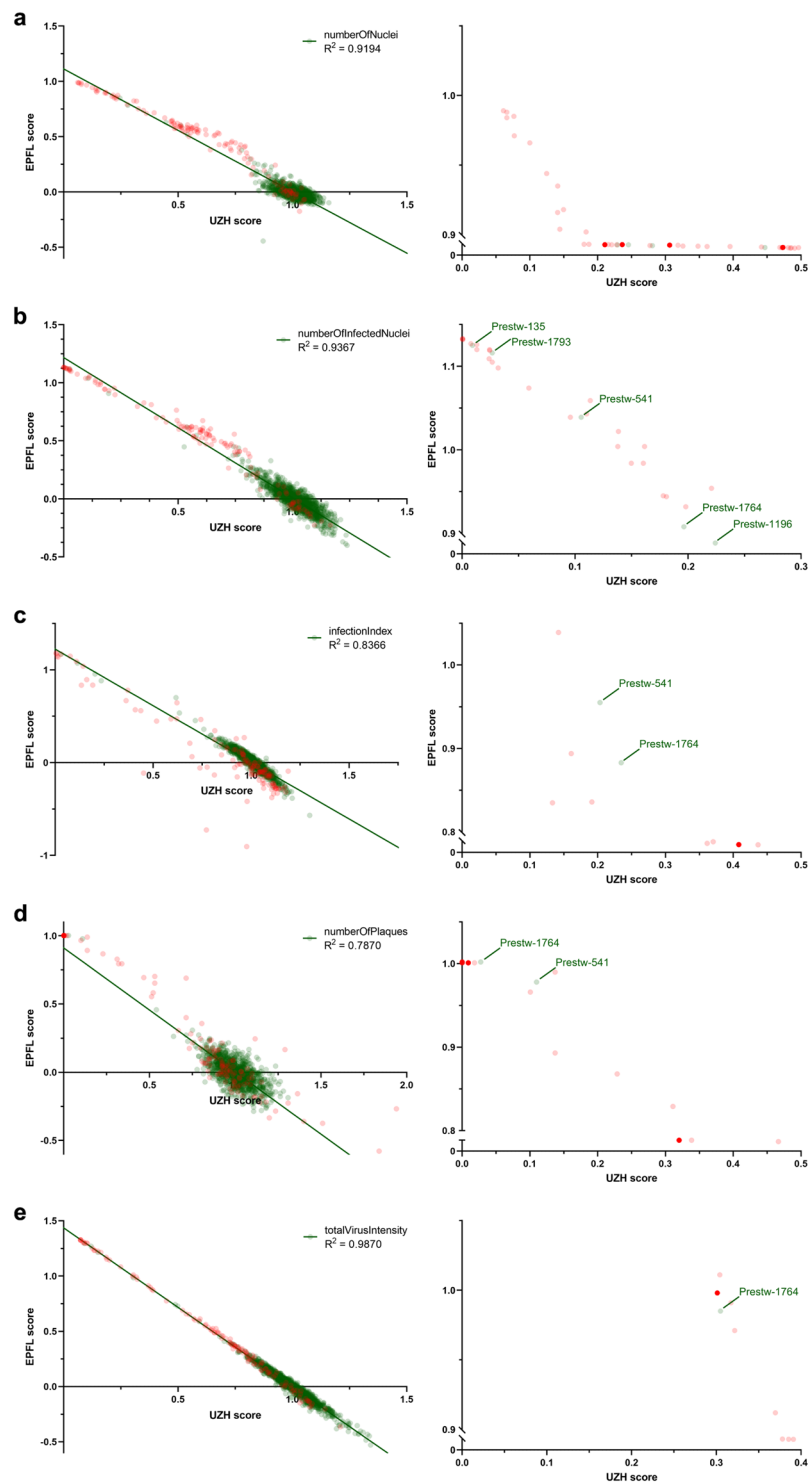


Fig. 6 Infection scores from independent dry-lab pipelines. Imaging, image analysis and data processing were performed independently at UZH and EPFL. Infection phenotypes in PCL-treated cells of four biological replicates were averaged and normalized against the DMSO solvent control. Linear regression plots of UZH and EPFL data are shown for (a) *numberOfNuclei*, (b) *numberOfInfectedNuclei*, (c) *infectionIndex*, (d) *numberOfPlaques* and (e) *totalVirusIntensity* of the 1,278 tested PCL compounds from are (green line). Red dots indicate toxicity in the absence of infection. Non-toxic compounds are shown as green dots. R^2 was calculated using GraphPad Prism 8.2.1. Highest scoring compounds are shown on the right, including the *PCL_ID* of some non-toxic compounds.

Infection scoring using the Plaque2.0 GUI. A detailed manual for Plaque2.0 GUI-based infection phenotype scoring is available at plaque2.github.io/. No MATLAB license is necessary.

The following settings should be used:

Input/Output:

Processing folder: Path to folder containing the images (e.g. *idr0081/3-Screen/Data_EPFL/Screen/BSF018292_1A*).

filename pattern Data_UZH: * (? < wellName > [A-Z][0-9]*) (? < channelName > w[0-9]*).TIF

filename pattern Data_EPFL: * (? < wellName > [A-Z] - [0-9] +) [(J)fld 1 wv (? < channel > [A-Z]{4})].*.tif

Plate name: Name of the plate to be analysed (e.g. *BSF018292_1A*)

Result Output Folder: Path to the results folder in the respective data folder (e.g. *idr0081/3-Screen/Data_EPFL/Results*).

Stitch: Stitching of the images is not necessary, since every 384-well is imaged in a single site. Do not activate the tab.

Mask:

Custom Mask File: Path to the manually defined mask file (e.g. *idr0081/3-Screen/Data_UZH/Parameters*). Well masking is optional and was not performed by EPFL.

Monolayer:

Channel: Nuclei were imaged in channel 1.

Plaque:

Channel: Viral GFP reporter signal was imaged in channel 2.

Infection scoring using the Plaque2.0 batch script. How to use the *AntiVir_batchprocessing.m* for Plaque2.0 batch processing is indicated in the comments of the code.

Code availability

Plaque2.0 batch image analysis for infection scoring. The MATLAB (version R2016b, The MathWorks, Natick, USA) script *AntiVir_batchprocessing.m* used by UZH for image analysis is provided for download at IDR, accession number *idr0081*, under *idr0081/3-Screen/Analysis*. It is based on the Plaque2.0 software available on GitHub under GPLv3 open source license: <https://github.com/plaque2/matlab>.

To batch analyse the HAdV screening data by Plaque2.0, fork or download the Plaque2.0 AntiVir code from GitHub: <https://github.com/plaque2/matlab/tree/antivir>. Place the *AntiVir_batchprocessing.m* file from *idr0081/3-Screen/Analysis* into the *Plaque2/matlab* folder and follow the instructions in *AntiVir_batchprocessing.m*. A MATLAB license is required.

Hit filtering using R. The R³⁹ (version 3.6.1 (2019-07-05)) script *AntiVir_hitfiltering.R* used by UZH for data processing and hit filtering is provided at IDR accession number *idr0081* under *idr0081/3-Screen/Analysis*.

Received: 18 May 2020; Accepted: 16 July 2020;

Published online: 12 August 2020

References

- Krilov, L. R. Adenovirus infections in the immunocompromised host. *Pediatr Infect Dis J* **24**, 555–556 (2005).
- Greber, U. F., Arnberg, N., Wadell, G., Benkő, M. & Kremer, E. J. Adenoviruses - from pathogens to therapeutics: a report on the 10th International Adenovirus Meeting. *Cell Microbiol* **15**, 16–23 (2013).
- Tunkel, A. R., Baron, E. L., Buch, K. A., Marty, F. M. & Martinez-Lage, M. Case 31-2019: A 45-Year-Old Woman with Headache and Somnolence. *N Engl J Med* **381**, 1459–1470 (2019).
- Gray, G. C. *et al.* Genotype prevalence and risk factors for severe clinical adenovirus infection, United States 2004–2006. *Clin Infect Dis* **45**, 1120–1131 (2007).
- Metzgar, D. *et al.* Abrupt emergence of diverse species B adenoviruses at US military recruit training centers. *J Infect Dis* **196**, 1465–1473 (2007).
- Lynch, J. P. & Kajon, A. E. Adenovirus: epidemiology, global spread of novel serotypes, and advances in treatment and prevention. *Semin Respir Crit Care Med* **37**, 586–602 (2016).
- Haque, E., Banik, U., Monowar, T., Anthony, L. & Adhikary, A. K. Worldwide increased prevalence of human adenovirus type 3 (HAdV-3) respiratory infections is well correlated with heterogeneous hypervariable regions (HVRs) of hexon. *PLoS ONE* **13**, e0194516 (2018).
- Jiang, H. *et al.* Oncolytic adenovirus research evolution: from cell-cycle checkpoints to immune checkpoints. *Curr Opin Virol* **13**, 33–39 (2015).
- Lawler, S. E., Speranza, M.-C., Cho, C.-F. & Chiocca, E. A. Oncolytic viruses in cancer treatment: A review. *JAMA Oncology* **3**, 841–849 (2017).
- Ginn, S. L., Amaya, A. K., Alexander, I. E., Edelstein, M. & Abedi, M. R. Gene therapy clinical trials worldwide to 2017: An update. *J Gene Med* **20**, e3015 (2018).
- Mennechet, F. J. D. *et al.* A review of 65 years of human adenovirus seroprevalence. *Expert Rev Vaccines* **18**, 597–613 (2019).
- Lion, T. Adenovirus persistence, reactivation, and clinical management. *FEBS Lett*, <https://doi.org/10.1002/1873-3468.13576> (2019).
- Ismail, A. M. *et al.* Genomic foundations of evolution and ocular pathogenesis in human adenovirus species D. *FEBS Lett* **593**, 3583–3608 (2019).
- Harrach, B., Tarján, Z. L. & Benkő, M. Adenoviruses across the animal kingdom: a walk in the zoo. *FEBS Lett*, <https://doi.org/10.1002/1873-3468.13687> (2019).
- Reddy, V. S., Natchiar, S. K., Stewart, P. L. & Nemerow, G. R. Crystal structure of human adenovirus at 3.5 Å resolution. *Science* **329**, 1071–1075 (2010).
- Benevento, M. *et al.* Adenovirus composition, proteolysis, and disassembly studied by in-depth qualitative and quantitative proteomics. *J Biol Chem* **289**, 11421–11430 (2014).
- Greber, U. F. & Flatt, J. W. Adenovirus entry: from infection to immunity. *Annual review of virology* **6**, 177–197 (2019).
- Bauer, M. *et al.* The e3 ubiquitin ligase mind bomb 1 controls adenovirus genome release at the nuclear pore complex. *Cell Rep* **29**, 3785–3795.e8 (2019).
- Greber, U. F. Virus and host mechanics support membrane penetration and cell entry. *J Virol* **90**, 3802–3805 (2016).

20. Wang, I.-H., Burckhardt, C. J., Yakimovich, A., Morf, M. K. & Greber, U. F. The nuclear export factor CRM1 controls juxta-nuclear microtubule-dependent virus transport. *J Cell Sci* **130**, 2185–2195 (2017).
21. Prasad, V. *et al.* The UPR sensor IRE1 α and the adenovirus E3-19K glycoprotein sustain persistent and lytic infections. *Nat Commun* **11**, 1997 (2020).
22. King, C. R., Zhang, A., Tessier, T. M., Gameiro, S. F. & Mymryk, J. S. Hacking the cell: network intrusion and exploitation by adenovirus E1A. *MBio* **9**, (2018).
23. Zheng, Y., Stamminger, T. & Hearing, P. E2f/rb family proteins mediate interferon induced repression of adenovirus immediate early transcription to promote persistent viral infection. *PLoS Pathog* **12**, e1005415 (2016).
24. Yakimovich, A. *et al.* Cell-free transmission of human adenovirus by passive mass transfer in cell culture simulated in a computer model. *J Virol* **86**, 10123–10137 (2012).
25. Tollefson, A. E. *et al.* The adenovirus death protein (E3-11.6K) is required at very late stages of infection for efficient cell lysis and release of adenovirus from infected cells. *J Virol* **70**, 2296–2306 (1996).
26. Doronin, K. *et al.* Overexpression of the ADP (E3-11.6K) protein increases cell lysis and spread of adenovirus. *Virology* **305**, 378–387 (2003).
27. Lenaerts, L. & Naesens, L. Antiviral therapy for adenovirus infections. *Antiviral Res* **71**, 172–180 (2006).
28. Wold, W. S. M., Tollefson, A. E., Ying, B., Spencer, J. F. & Toth, K. Drug development against human adenoviruses and its advancement by Syrian hamster models. *FEMS Microbiol Rev* **43**, 380–388 (2019).
29. Georgi, F. *et al.* High-content image-based drug screen identifies a clinical compound against cell transmission of adenovirus. *figshare* <https://doi.org/10.6084/m9.figshare.c.5052965> (2020).
30. Chauvin, C. *et al.* High-Throughput Drug Screening Identifies Pazopanib and Clofilium Tosylate as Promising Treatments for Malignant Rhabdoid Tumors. *Cell Rep* **21**, 1737–1745 (2017).
31. Wall, G. *et al.* Screening a Repurposing Library for Inhibitors of Multidrug-Resistant *Candida auris* Identifies Ebselen as a Repositionable Candidate for Antifungal Drug Development. *Antimicrob Agents Chemother* **62** (2018).
32. Yakimovich, A. *et al.* Plaque2.0-A High-Throughput Analysis Framework to Score Virus-Cell Transmission and Clonal Cell Expansion. *PLoS ONE* **10**, e0138760 (2015).
33. Georgi, F. *et al.* High-content image-based drug screen identifies a clinical compound against cell transmission of adenovirus. *University of Dundee* <https://doi.org/10.17867/10000136> (2020).
34. Georgi, F. *et al.* The FDA-approved drug Nelfinavir inhibits lytic cell-free, but not cell-associated non-lytic transmission of human adenovirus. *Antimicrob Agents Chemother*, <https://doi.org/10.1128/AAC.01002-20> (2020).
35. Georgi, F. *et al.* Mutant Human adenovirus 2 isolate HAdV-C2-dE3B-CMV-GFP, complete sequence. *GenBank* <https://identifiers.org/ncbi/insdc:MT277585.1> (2020).
36. Greber, U. F., Willetts, M., Webster, P. & Helenius, A. Stepwise dismantling of adenovirus 2 during entry into cells. *Cell* **75**, 477–486 (1993).
37. Boncler, M., Różalski, M., Krajewska, U., Podśedek, A. & Watala, C. Comparison of PrestoBlue and MTT assays of cellular viability in the assessment of anti-proliferative effects of plant extracts on human endothelial cells. *J Pharmacol Toxicol Methods* **69**, 9–16 (2014).
38. Xu, M., McCanna, D. J. & Sivak, J. G. Use of the viability reagent PrestoBlue in comparison with alamarBlue and MTT to assess the viability of human corneal epithelial cells. *J Pharmacol Toxicol Methods* **71**, 1–7 (2015).
39. R Core Team. *R: A Language and Environment for Statistical Computing*. (R Foundation for Statistical Computing, 2018).
40. Berthold, M. R. *et al.* KNIME - the Konstanz information miner. *ACM SIGKDD Explorations Newsletter* **11**, 26 (2009).

Acknowledgements

We thank the Greber lab for fruitful discussions and critical assessment of the data. We thank the IDR team for helping to make our work openly accessible. The work was supported by the Swiss National Science Foundation (SNSF) to U.F.G. (Grant numbers 316030_170799/1 and 31003A_179256/1), and the SNSF National Research Program “NCCR Chemical Biology” to G.T. and U.F.G.

Author contributions

U.F.G., V.A., A.Y. conceived the screening idea. F.G. designed the experiments, and with U.F.G. coordinated the project. F.K. prepared the PCL-spotted plates. F.G. and R.W. performed the experiments. F.G. and F.K. acquired the data. F.G. and V.A. analysed the imaging data. L.M. and F.G. processed the data. G.T. organized and supervised the screening project at the EPFL-BSF. F.G., F.K. and U.F.G. wrote manuscript, with input from all the co-authors.

Competing interests

The authors declare no competing interests.

Additional information

Correspondence and requests for materials should be addressed to U.F.G.

Reprints and permissions information is available at www.nature.com/reprints.

Publisher's note Springer Nature remains neutral with regard to jurisdictional claims in published maps and institutional affiliations.



Open Access This article is licensed under a Creative Commons Attribution 4.0 International License, which permits use, sharing, adaptation, distribution and reproduction in any medium or format, as long as you give appropriate credit to the original author(s) and the source, provide a link to the Creative Commons license, and indicate if changes were made. The images or other third party material in this article are included in the article's Creative Commons license, unless indicated otherwise in a credit line to the material. If material is not included in the article's Creative Commons license and your intended use is not permitted by statutory regulation or exceeds the permitted use, you will need to obtain permission directly from the copyright holder. To view a copy of this license, visit <http://creativecommons.org/licenses/by/4.0/>.

The Creative Commons Public Domain Dedication waiver <http://creativecommons.org/publicdomain/zero/1.0/> applies to the metadata files associated with this article.

© The Author(s) 2020